Transmon Qubits

Kadircan Godeneli* and Elias Lehman†

(Dated: May 13, 2023)

Superconducting qubits provide one of the most promising platforms to realize a large-scale fault-tolerant quantum computer. This project comprehensively reviews its fundamental building block, namely the transmon qubit, and its underlying math and physics. In particular, we will start with the basics of the transmon. We will then discuss the design, control, and readout schemes of superconducting qubits in detail. Finally, building upon these fundamentals, we will cover the challenges in state-of-the-art superconducting qubit research, such as the limiting factors of qubit lifetime, and discuss approaches taken to overcome this problem.

I. CONTRIBUTION STATEMENT

Abstract, Section II, and and Section IV-C were written together. Section III, and Section IV-A & B were written by Elias. Section IV-D & E & F, Section V, and Appendix were written by Kadircan.

II. INTRODUCTION

Superconducting LC resonators have equally spaced energy spectra, which are not suitable to store quantum information. With the introduction of a nonlinear inductive element, the Josephson Junction, an anharmonic quantum oscillator is achieved so that the two lowest energy states can be isolated as the computational subspace, making an artificial atom out of electrical circuits, known as superconducting qubits. In particular, the transmon qubit, the most popular type of superconducting qubit, has sufficiently large anharmonicity, while exponentially suppressing charge dispersion, enabling significantly higher coherence. Thanks to the invention of the transmon qubit, superconducting qubits are a cornerstone technology of quantum computing, and continue to grow in popularity. Since the first demonstration of charge qubits in 1999 [1], quantum processors using superconducting qubits have shown exemplary progress in their coherence times, number of qubits, controllability, and readout.

The motivation is due to the fact that although there has been significant improvement in the qubit lifetime, it has been more or less saturated at around a few hundred microseconds recently. Quantum error correction can protect quantum computations from physical errors by encoding logical qubits into many physical qubits. However, physical qubit error rates must be sufficiently low to minimize resource overhead, and suppress errors. As a result, improving qubit lifetime, which is important to achieve low qubit gate error rates, is an active challenge in the scientific community, since realizing a fault-tolerant large-scale quantum computer will be enabled with better physical qubits. In this project, we will study the original transmon paper, review papers covering superconducting qubits and circuit quantum electrodynamics, and select papers from the literature on state-of-the-art implementations of transmon qubits. In particular, we will analyze what approaches are taken in the literature to improve superconducting qubit lifetimes for large scale superconducting quantum processors. These include the use of improved materials, advanced qubit architectures, and microwave engineering.

III. BACKGROUND

This section covers literature review in transmon qubit engineering. The intent of this section is to direct the curious reader to external references which are key influences in the writing of this paper.

A. Superconductivity

Throughout this work, it is assumed that circuits are operated at low enough temperatures such that the materials of which they are composed are in a superconducting phase. Superconductivity in this definition implies that supercurrent flows without resistive dissipation of energy. The physics of superconductivity is a very rich subject, and further questions are being investigated as for how different superconductive states affect the behavior of qubits. The specific superconductive behavior assumed in this paper is based on Bardeen, Cooper, and Schrieffer (BCS) theory, or Type 1 superconductivity. The curious reader should see the original paper by Bardeen, Cooper, and Schrieffer [2], and the textbook [3].

B. The Transmon Qubit

Origins of the transmon qubit date to the 2007 paper by Koch *et al.* titled *Charge-insensitive qubit design derived from the Cooper pair box.* Yale professors S. M. Girvin, M. H. Devoret, and R. J. Schoelkopf were the principal investigators behind this work which

---

* University of California, Berkeley; kadircan@berkeley.edu
† University of California, Berkeley; eliaslehman@berkeley.edu

built upon their shared background in quantum information theory [4], quantum coherence of single cooper pairs [5], cavity quantum electrodynamics (cQED) [6], and qubit noise spectrometers [7]. The paper defines and highlights the importance of the Transmon Regime, a ratio of the Josephson energy to the charging energy ($E_J/E_C >> 1$), required to suppress charge dispersion exponentially, while reducing anharmonicity by a linear power law.

C. Scaling Quantum Integrated Circuits; The Xmon Geometry

The underlying motivation for studying qubits is the development of large-scale, fault tolerant quantum computers. This leads to many questions about designing the qubit geometry, and in the case of superconducting qubits, it introduces questions as to how we can incorporate qubits into modern day integrated circuits. Barends et al. presented the 'Xmon' qubit shown in Fig. 1 in 2013, paving a way for easily connected designs of superconducting quantum processors [8]. The design included a cross shaped qubit capacitor with coupling capacitances on each end, leading to control and readout lines and a nearby Josephson Junction with a frequency tunable SQUID (superconducting quantum interference device) loop. This modular design, named after the cross feature, is now a popular design used in the field.
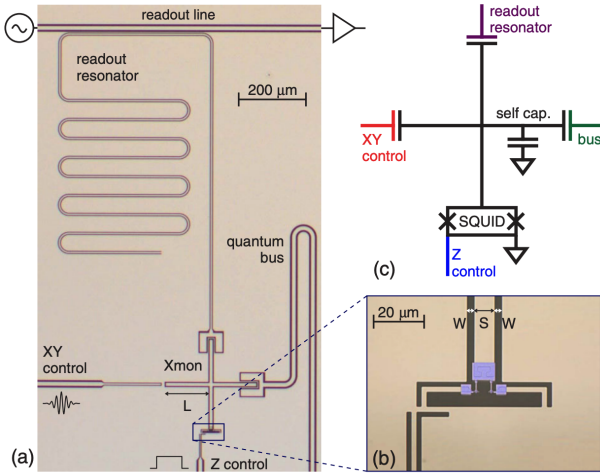

FIG. 1. (a) Layout of 'Xmon' qubit, with control line to the left, readout line and resonator near the top, SQUID at the bottom, and quantum bus for qubit-qubit coupling to the right. Generally, low coupling is desired at the XY control line to reduce energy leakage, whereas high coupling to the readout line is desired for high fidelity phase reflection during measurement. (b) Equivalent circuit diagram. (c) SQUID loop with Josephson Junctions. Figure taken from [8].

D. High Fidelity Gates & Measurements

In 2013, Gustavsson et al. used a novel approach to measure superconducitng qubit control distortions, effectively reducing the average error per gate by 37 per cent, achieving single gate fidelities as high as 99.8 per cent [9]. In April of 2014, Barends et al. claimed that superconducting quantum processors were on the brink of the fault-tolerance threshold for surface code error correction, reporting an average single-qubit gate fidelity of 99.92 per cent and a two-qubit gate fidelity of up to 99.4 per cent [10]. The methods for achieving these fidelities are similar to those covered in this report however the origins of this technology may be found in the aforementioned papers.

A standard readout scheme is also covered in this report. To measure the state of a superconducting qubit, a readout pulse is applied through an input line with attenuators that reduce the noise from room temperature instruments to single microwave photon level. The pulse is directed via a microwave circulator, reflected with a phase shift, or frequency shift in the readout resonator based on the state of the qubit, before passing through isolators to protect against output chain noise. The pulse is amplified at the 4 K stage and again at room temperature before being digitized. Improvements have been made in last 15 years with the desire of quantum computation which employs feedback and dynamic state-dependent operations [11]. Such improvements include the addition of a Purcell filter in 2010 which reduces relaxation via spontaneous emission [12], a Josephson Parametric Circuit first demonstrated in 2013 used to amplify the reflected signal with less than 1.5 photons of noise [13], and FPGA control electronics which enable low-latency signal processing in hardware.

IV. THEORY

A. Quantum LC Resonator

It is natural to begin this paper with a review of the LC oscillator circuit, on which superconducting qubit architectures are based on. In terms of the charge on the capacitor q, and the current through the inductor I

$$\mathcal{L} = \frac{1}{2}LI^2 - \frac{1}{2}\frac{q^2}{C} = \frac{1}{2}L\dot{q}^2 - \frac{1}{2}\frac{q^2}{C} \qquad (1)$$

which yielded the Euler-Lagrange equation $\ddot{q} = -\Omega^2 q$ where we define the natural oscillation frequency to be

$$\Omega = \frac{1}{\sqrt{LC}} \qquad (2)$$

The conjugate momentum to the charge coordinate is the flux through the inductor.

$$\Phi = \frac{\delta\mathcal{L}}{\delta\dot{q}} = LI \qquad (3)$$

$$\therefore H = \Phi q - \mathcal{L} = \frac{\Phi^2}{2L} + \frac{q^2}{2C} \qquad (4)$$

Hamilton's equations of motion give the current through the inductor and voltage at the node connecting the inductor and capacitor

$$\dot{q} = \frac{\partial H}{\partial \Phi} = \frac{\Phi}{L} = I \qquad (5)$$

$$\dot{\Phi} = -\frac{\partial H}{\partial q} = -\frac{q}{C} = V \qquad (6)$$

In their quantum operator form, charge and flux obey the canonical commutation relation $[\hat{\Phi}, \hat{q}] = -i\hbar$. Thus, we can define annihilation and creation operators

$$\hat{\alpha} = +i\frac{\hat{\Phi}}{\sqrt{2L\hbar\omega_0}} + \frac{\hat{Q}}{\sqrt{2C\hbar\omega_0}} \qquad (7)$$

$$\hat{\alpha}^\dagger = -i\frac{\hat{\Phi}}{\sqrt{2L\hbar\omega_0}} + \frac{\hat{Q}}{\sqrt{2C\hbar\omega_0}} \qquad (8)$$

$$\therefore H = \frac{\hbar\omega_0}{2}(\hat{\alpha}^\dagger\hat{\alpha} + \hat{\alpha}\hat{\alpha}^\dagger) = \hbar\omega_0(\hat{\alpha}^\dagger\hat{\alpha} + \frac{1}{2}) \qquad (9)$$

Thus far, we have successfully derived the Hamiltonian for the LC resonator, which resembles the quantum harmonic oscillator with q as our coordinate of choice and Φ as its conjugate momentum. However, in the context of the Josephson junction, our LC resonator will have a non-linear inductance, so it will be more convenient to choose the flux as the coordinate. Performing a change of basis, we have

$$\mathcal{L} = \frac{1}{2}C\dot{\Phi}^2 - \frac{1}{2}\frac{\Phi^2}{L} \qquad (10)$$

It's important to remember that in this new basis we must maintain the commutation relation between our coordinate $\hat{\Phi}$ and its conjugate momentum, denoted $\hat{Q}$. As we have chosen to keep $\hat{\Phi}$ consistent, we must let $\hat{Q} = -\hat{q}$, but this only results in a couple negations during the derivation, and no meaningful difference in the equation and of course not in the underlying physics.

Using a similar procedure as before, we have

$$H = Q\dot{\Phi} - \mathcal{L} = \frac{Q^2}{2C} + \frac{\Phi^2}{2L} \qquad (11)$$

$$\dot{\Phi} = +\frac{\partial H}{\partial Q} = \frac{Q}{C} = V \qquad (12)$$

$$\dot{Q} = -\frac{\partial H}{\partial \Phi} = -\frac{\Phi}{L} = -I \qquad (13)$$

as we expect.

The new annihilation and creation operators become

$$\hat{\alpha} = +i\frac{\hat{Q}}{\sqrt{2C\hbar\omega_0}} + \frac{\hat{\Phi}}{\sqrt{2L\hbar\omega_0}} \qquad (14)$$

$$\hat{\alpha}^\dagger = -i\frac{\hat{Q}}{\sqrt{2C\hbar\omega_0}} + \frac{\hat{\Phi}}{\sqrt{2L\hbar\omega_0}} \qquad (15)$$

such that the Hamiltonian in terms of these operators remains Eq (9).

Furthermore, we can express the charge and flux operators in terms of the creation and annihilation operators in an elegant way which incorporates the characteristic impedance, Z, of the oscillator:

$$\hat{Q} = -iQ_{ZPF}(\hat{\alpha} - \hat{\alpha}^\dagger) \qquad (16)$$

$$\hat{\Phi} = -i\Phi_{ZPF}(\hat{\alpha} + \hat{\alpha}^\dagger) \qquad (17)$$

where

$$Q_{ZPF} = \sqrt{\frac{C\hbar\Omega}{2}} = \sqrt{\frac{\hbar}{2Z}} \qquad (18)$$

$$\Phi_{ZPF} = \sqrt{\frac{L\hbar\Omega}{2}} = \sqrt{\frac{\hbar Z}{2}} \qquad (19)$$

for $Z = \sqrt{\frac{L}{C}}$ as in the classical LC oscillator.

We have chosen to define Q_{ZPF} and Φ_{ZPF} in such a way that they represent **the quantum ground state uncertainties** in charge and flux. Naturally, they obey the usual uncertainty principle

$$Q_{ZPF}\Phi_{ZPF} = \frac{\hbar}{2} \qquad (20)$$

Hereafter, we will use the dimensionless characteristic impedance $z = Z \times 2G_0$, instead of Z. G_0 is the conductance quantum, $G_0 = \frac{2e^2}{h} \approx 7.74809 \times 10^{-5}$ S which describes the conductance of two quantum channels (one for spin up and one for spin down) when the probability for transmitting an electron that enters the channel is unity, i.e. during ballistic transport or superconductive states.

We see that

$$Q_{ZPF} = (2e)\sqrt{\frac{1}{4\pi z}} \qquad (21)$$

$$\Phi_{ZPF} = \Phi_0\sqrt{\frac{z}{4\pi}} \qquad (22)$$

where

$$\Phi_0 \equiv \frac{h}{2e} \qquad (23)$$

is the superconducting flux quantum; h and e are the Planck constant and electron charge, respectively.

B. Josephson Junctions

A single Josephson Junction, shown in Fig. 2, is able to coherently transfer Cooper pairs from one superconducting island to another via quantum tunneling. This simplified description is known as the Cooper Pair Box (CPB), and is a foundational example to understand the behavior of Josephson Junctions in the context of superconducting qubits.

Consider a Type 1 superconductor (one that follows BCS theory, such as cryogenically cooled Al). In this phase, electrons of spin-up and spin-down join together to form Cooper pairs of lower ground state. This ground state is unique, non-degenerate, and separated from the excited states by a gap of 2Δ, where Δ is the energy required to break a Cooper pair, on the order of several kelvin (multiplied by the Boltzmann constant).
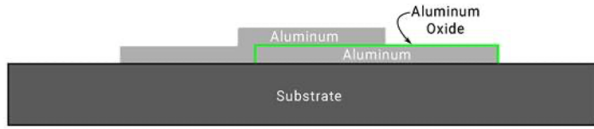

FIG. 2. Common architecture of Josephson Junction. Superconducting aluminum electrodes are separated by a thin layer of insulating aluminum oxide, forming a tunnel junction.

Consider two superconducting islands separated by a thin insulating barrier. Assume that the total number of electron pairs in a system is fixed to some $N = N_1 + N_2$. Ignoring the Coulomb energy of the newly formed capacitor, the total number of pairs no longer uniquely defines the quantum state. There is now a family of degenerate ground states which we will denote as

$$|m\rangle = |N_1 - m, N_2 + m\rangle \tag{24}$$

Now consider the resulting Hamiltonian

$$H_T = -\frac{1}{2} E_J \sum_m (|m\rangle \langle m+1| + |m+1\rangle \langle m|) \tag{25}$$

where E_J is the Josephson coupling energy, a measure of the ability of Cooper pairs to tunnel through the barrier. The Josephson energy is approximated by the Ambegaokar-Baratoff relation

$$E_J = G_0 G_N \Delta \tag{26}$$

where $G_N = \frac{1}{R_N}$ is the normal state conductance which is calculated using Fermi's Golden Rule for the tunneling rate.

The Hamiltonian H_T connects a set of discrete states resulting in coherent tunneling, as mentioned at the beginning of this section. The solution to the Schrödinger equation for such a Hamiltonian is found via degenerate perturbation theory to be

$$|\varphi\rangle = \sum_m e^{im\varphi} |m\rangle \tag{27}$$

with eigenvalues given by

$$H_T |\varphi\rangle = -E_J \cos \varphi |\varphi\rangle. \tag{28}$$

The current flowing through the junction is given by calculating the group velocity of such a wave packet

$$v_g(\varphi) = \frac{1}{\hbar} \frac{\partial}{\partial \varphi} [-E_J \cos \varphi] \tag{29}$$

$$\therefore I(\varphi) = -2e v_g(\varphi) = \frac{2e}{\hbar} E_J \sin \varphi \tag{30}$$

Let the critical current, above which will result in ohmic behavior, be denoted

$$I_c = \frac{2e}{\hbar} E_J. \tag{31}$$

In the case of a voltage applied across the junction, we add a potential term

$$U = -(2e)V\hat{n} \tag{32}$$

to the Hamiltonian, where

$$\hat{n} \equiv \sum_m |m\rangle m \langle m| \tag{33}$$

be the operator which gives the number of charges crossing the junction.

The Hamiltonian with this new term is given by

$$H = -E_J \cos \varphi - 2eV\hat{n} \tag{34}$$

C. The Transmon Regime

The previous section purposefully ignored the Coulomb interaction resulting from the capacitance of the Josephson Junction. When we shunt the Junction with a large capacitor, we can define the charging energy associated with transfer of a single electron

$$E_C = \frac{e^2}{2C_\Sigma} \tag{35}$$

where $C_\Sigma = C_J + C_g$ is the total capacitance between the Josephson Junction C_J and the gate capacitance C_g (See Fig. 5). Transfer of a Cooper pair requires four times this energy, so the operator is given by

$$\hat{U} = 4E_C(\hat{n} - n_g)^2 \tag{36}$$

for gate charge

$$n_g \equiv -\frac{C_g V}{2e} \tag{37}$$

which represents the effect of an external electric field that breaks degeneracy. As a continuous variable, the fluctuations of n_g can be considered a source of noise.

Incorporating these terms into the Hamiltonian of the Josephson Junction alone, we arrive at

$$H = 4E_C(\hat{n} - n_g)^2 - E_J \cos\hat{\varphi} \qquad (38)$$

The reader should closely examine this Hamiltonian side-by-side with that of a rigid rotor (See Givin's notes in [14] for more detail). Noticing the similarity, we can make a powerful analogy resulting in an interesting approximation. In the case of small amplitudes, the rigid rotor can be closely approximated by the harmonic oscillator, but in the limit of large amplitudes, its behavior diverges. Similarly, Eq (38) exhibits the behavior analogous to the harmonic oscillator when the cosine term is expanded to second order, a valid approximation only if $E_J >> E_C$. We call the ratio of $E_J/E_C >> 1$, in which this is a valid approximation, the **transmon regime**. The Hamiltonian in this case is given by

$$H \approx 4E_C\hat{n}^2 + \frac{1}{2}E_J\hat{\varphi}^2 \qquad (39)$$

Further, we can connect this Hamiltonian directly to that of the LC resonator studied in subsection A. Notice that in the case of the quantum LC resonator, the phase angle φ may be expressed as

$$\varphi = \frac{2e}{\hbar}\Phi = 2\pi\frac{\Phi}{\Phi_0} \qquad (40)$$

For each increase of the flux by one flux quantum, the superconducting phase experiences a full rotation. This leads to the Lagrangian for the CPB

$$\mathcal{L} = \frac{1}{2}C\dot{\Phi}^2 + E_J\cos\left(2\pi\frac{\Phi}{\Phi_0}\right) \qquad (41)$$

Expanding the cosine term about $\Phi = 0$ to lowest order gives

$$\mathcal{L} = \frac{1}{2}C\dot{\Phi}^2 - \frac{1}{2L_J}\Phi^2 \qquad (42)$$

where the effective inductance of the Josephson junction is given by

$$L_J = (\frac{\hbar}{2e})^2\frac{1}{E_J} \qquad (43)$$

In this approximation, the resonant frequency of the CPB is

$$\Omega_J \equiv \frac{1}{\sqrt{L_JC}} = \frac{1}{\hbar}\sqrt{8E_JE_C} \qquad (44)$$

Leaving the harmonic approximation, we see that for general flux Φ, we can define the differential inductance as

$$L(\Phi) \equiv (\frac{d^2H}{d\Phi^2})^{-1} = (E_J(\frac{2\pi}{\Phi_0})^2\cos\left(2\pi\frac{\Phi}{\Phi_0}\right))^{-1} \qquad (45)$$

thus, **the Josephson junction is a non-linear inductor**.

To further see the impact of the transmon regime, we make another analogy, this time to the band structure of a one-dimensional solid with a cosine potential in which the offset charge defines the Bloch wavevector $-\frac{1}{2} \leq k \leq \frac{1}{2}$ for wavefunction

$$\Psi_{mk}(\varphi) = e^{ik\varphi}\psi_m(\varphi). \qquad (46)$$

In this picture, representative of near-neighbor hopping in a tight-binding model, the eigenvalues for such eigenvector are [15]

$$E_m(n_g) \approx E_m + \epsilon_m\cos(2\pi n_g) \qquad (47)$$

where ϵ_m defines the 'charge-dispersion'. In the WKB approximation of this model, the charge dispersion is explicitly given by [15]

$$\epsilon_m \approx (-1)^m E_C\frac{2^{4m+5}}{m!}(\frac{E_J}{2E_C})^{\frac{m}{2}+\frac{3}{4}}e^{-\sqrt{8E_J/E_C}} \qquad (48)$$

Charge dispersion measures the sensitivity of the energy levels to the offset charge. We see that it has an inverse exponential dependence on $\sqrt{E_J/E_C}$. Going to the transmon regime, large E_J/E_C, makes the qubit highly insensitive to low-frequency charge noise, dramatically improving dephasing time. This insensitivity can be seen in Fig. 3 where subfigure (d) corresponds to the transmon regime with $E_J/E_C = 50$. We have also numerically simulated the first 4 energy levels of transmon for $E_J/E_C = 5$ and $E_J/E_C = 50$ as a function of offset charge n_g, which can be seen in the Appendix A, using sc-Qubits Python package [16].

Furthermore, we define the anharmonicity as $\alpha \equiv E_{12} - E_{01}$ where $E_{12} = E_2 - E_1$ and $E_{01} = E_1 - E_0$. Recall the Hamiltonian $H = 4E_C(\hat{n} - n_g)^2 - E_J\cos\hat{\varphi}$. We can expand the cosine term around $\varphi = 0$ up to the fourth order $\cos\varphi \approx 1 - \frac{1}{2!}\varphi^2 + \frac{1}{4!}\varphi^4$. Then, the fourth order term, which is the perturbation to the harmonic oscillator, is $V = -\frac{E_J}{4!}\hat{\varphi}^4$. Substituting $\hat{\varphi} = \varphi_{ZPF}(\hat{a} + \hat{a}^\dagger)$ where $\varphi_{ZPF} = (\frac{2E_C}{E_J})^{1/4}$, one obtains $V = -\frac{E_C}{12}(\hat{a} + \hat{a}^\dagger)^4$ [17]. We can now perform calculations with first-order perturbation theory to get the corrections for the energy levels.

$$E_j^{(1)} = \langle j|V|j\rangle = -\frac{E_C}{12}\langle j|(\hat{a} + \hat{a}^\dagger)^4|j\rangle \qquad (49)$$

where $|j\rangle$ is the harmonic oscillator eigenstates with no perturbation. Straightforward algebra yields

$$E_j^{(1)} = -\frac{E_C}{12}(6j^2 + 6j + 3) \qquad (50)$$

As a result, the eigenenergies can be written as

$$E_j = \hbar\Omega(j + \frac{1}{2}) - E_J - \frac{E_C}{12}(6j^2 + 6j + 3) \qquad (51)$$
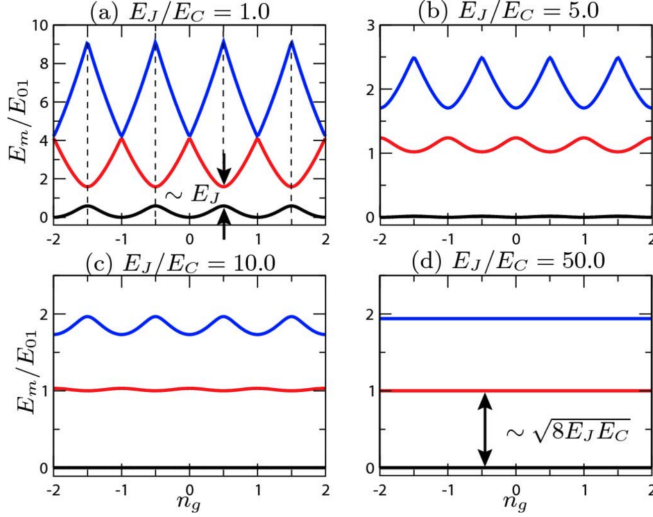
FIG. 3. Band diagram of ground, first, and second excited states versus charge offset. Notably, increasing E_J/E_C flattens the bands, implying a reduction in sensitivity to charge dispersion. Figure taken from [15].

where $\Omega = \frac{\sqrt{8E_J E_C}}{\hbar}$. We can calculate $E_{12} = E_2 - E_1 = \hbar\Omega - 2E_C$ and $E_{01} = E_1 - E_0 = \hbar\Omega - E_C$. Then, the anharmonicity can be calculated as

$$\alpha = E_{12} - E_{01} = -E_C \tag{52}$$

Moreover, the relative anharmonicity can be written

$$\alpha_r \equiv \alpha/E_{01} \tag{53}$$

where $E_{01} = \hbar\Omega = \sqrt{8E_J E_C}$. Finally,

$$\alpha_r = -E_C/\sqrt{8E_J E_C} = -(8E_J/E_C)^{-1/2} \tag{54}$$

which is a function of the ratio E_J/E_C.

Note that anharmonicity depends on E_J/E_C with a weak power law such that we still have sufficiently large anharmonicity in the transmon regime, while the sensitivity to charge noise is exponentially suppressed. In this regime, anharmonicity can easily be kept above an adequate level of 100-200 MHz to apply fast control pulses.

D. Qubit Control

Let us derive the formalism for the superconducting qubit drive with capacitive coupling, whose circuit diagram is shown in Fig. 4. Let us start by writing down the Lagrangian for the circuit diagram as

$$\mathcal{L} = \frac{1}{2}C\dot{\Phi}^2 - \frac{1}{2L}\Phi^2 + \frac{1}{2}C_d(\dot{\Phi} - V_d)^2 \tag{55}$$

where we define the flux as
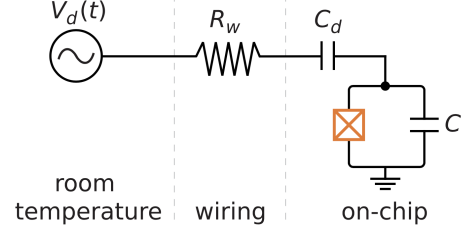
$$\Phi(t) = \int_0^t V(\tau)\,d\tau \tag{56}$$

FIG. 4. Circuit diagram of capacitive coupling of a microwave drive line to a superconducting qubit. Figure taken from [18].

For the moment, if we consider $V_d = 0$, we see that the conjugate momentum is

$$\frac{\partial \mathcal{L}}{\partial \dot{\Phi}} = (C + C_d)\dot{\Phi} = Q \tag{57}$$

which is the total charge at the capacitors. Here, we see the contribution from the C_d capacitor on top of the qubit capacitor. Then, upon Legendre transformation, the Hamiltonian without the drive can be written as

$$H = \frac{Q^2}{2(C + C_d)} + \frac{\Phi^2}{2L} \tag{58}$$

Now, let us revisit the initial Lagrangian we wrote $\mathcal{L} = \frac{1}{2}C\dot{\Phi}^2 - \frac{1}{2L}\Phi^2 + \frac{1}{2}C_d(\dot{\Phi} - V_d)^2$. We identify the drive contribution as $\mathcal{L}_d = -C_d\dot{\Phi}V_d(t)$, dropping the term $\frac{1}{2}C_d V_d^2$, since it is only a constant energy shift term that does not include any parameter dependency. Then, the drive Hamiltonian is

$$H_d = C_d\dot{\Phi}V_d = \frac{Q}{1 + C/C_d}V_d(t) \tag{59}$$

We can now write down the full Hamiltonian including the drive term

$$H = \frac{Q^2}{2(C + C_d)} + \frac{\Phi^2}{2L} + \frac{V_d(t)}{1 + C/C_d}Q \tag{60}$$

We can reexpress the charge Q in the language of creation and annihilation operations

$$Q = -iQ_{ZPF}(\hat{a} - \hat{a}^\dagger) \tag{61}$$

where $Q_{ZPF} = \sqrt{\frac{\hbar}{2Z}}$, $Z = \sqrt{\frac{L}{C+C_d}}$. Plugging these in, we obtain the expression for the drive Hamiltonian as

$$H_d = -i\frac{C_d}{C + C_d}V_d(t)Q_{ZPF}(\hat{a} - \hat{a}^\dagger) \tag{62}$$

and if we add the qubit, we obtain the full Hamiltonian as

$$H = -\frac{\omega_q}{2}\sigma_z + \Omega V_d(t)\sigma_y \tag{63}$$

where $\Omega = \frac{C_d}{C+C_d}Q_{ZPF}$, and $\omega_q = (E_1 - E_0)/\hbar$. Note that this Hamiltonian is time-dependent. We shall move

to the rotating frame to get rid of this time-dependency via the unitary transformation

$$e^{iH_0 t} = e^{-i\frac{\omega_q}{2}t\sigma_z} \tag{64}$$

Then, the drive Hamiltonian in the rotating frame (rf) is

$$H_{d,rf} = \Omega V_d(t)(\cos(\omega_q t)\sigma_y - \sin(\omega_q t)\sigma_x) \tag{65}$$

where σ_x and σ_y are Pauli X and Y matrices. Let us consider a drive voltage in the form $V_d(t) = V_0 v(t)$ where $v(t) = s(t)\sin(\omega_d t + \phi)$, or equivalently

$$v(t) = s(t)(\cos(\phi)\sin(\omega_d t) + \sin(\phi)\cos(\omega_d t)) \tag{66}$$

where $s(t)$ is a dimensionless envelope function. Let $I \equiv \cos(\phi)$, and $Q \equiv \sin(\phi)$, which are the in-phase, and out-of-phase components, respectively. We can then write the Hamiltonian as

$$H_{d,rf} = \Omega V_0 s(t)(I\sin(\omega_d t) - Q\cos(\omega_d t)) \\ \times (\cos(\omega_q t)\sigma_y - \sin(\omega_q t)\sigma_x) \tag{67}$$

Upon trigonometrical manipulation, and dropping fast oscillating terms, known as rotating wave approximation, we obtain

$$H_{d,rf} = \frac{1}{2}\Omega V_0 s(t)[(-I\cos(\delta\omega t) + Q\sin(\delta\omega t))\sigma_x \\ + (I\sin(\delta\omega t) - Q\cos(\delta\omega t))\sigma_y] \tag{68}$$

where $\delta\omega = \omega_q - \omega_d$ is the detuning. If we drive on resonance ($\delta\omega = 0$), drive Hamiltonian reduces down to

$$H_{d,rf} = -\frac{\Omega}{2}V_0 s(t)(I\sigma_x + Q\sigma_y) \tag{69}$$

where we see that in-phase and out-of-phase components perform rotations around x- and y-axes on the Bloch Sphere, respectively. To exemplify, we shall take a look at the case with in-phase component ($\phi = 0$). The unitary operator for this operation is

$$U_{d,rf}^{\phi=0}(t) = e^{\frac{i}{2}\Omega V_0(\int_0^t s(t')dt')\sigma_x} \tag{70}$$

where we see that pulse envelope function is integrated over time. We can write the rotation angle as

$$\Theta(t) = -\Omega V_0 \int_0^t s(t')dt' \tag{71}$$

To apply a π-pulse on the x-axis, one needs to achieve $\Theta(t) = \pi$. In summary, to perform rotations on the Bloch Sphere, one needs to send coherent microwave pulses that are near qubit transition frequency [14].

E. Circuit Quantum Electrodynamics

Circuit quantum electrodynamics (circuit QED) is a formalism that is analogous to cavity quantum electrodynamics. Circuit QED treats the superconducting qubit as an artificial atom with two energy levels, and the qubit is coupled to a linear microwave LC resonator which is the cavity in the context of cavity QED. Let us now derive the Jaynes-Cummings Hamiltonian, from which we shall derive the formalism for the dispersive readout of superconducting qubits.

The circuit model for a transmon qubit that is coupled to an LC resonator is shown in Fig. 5. The Hamiltonian
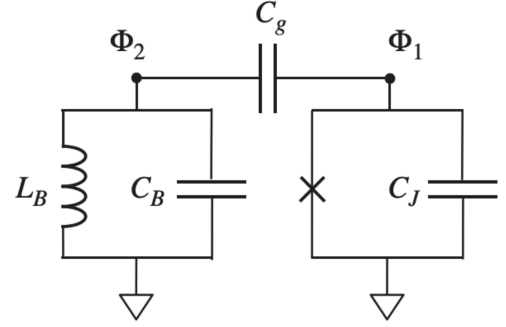

FIG. 5. Circuit model of a capacitively coupled qubit-resonator system. Figure taken from [14].

for the qubit part is

$$H_1 = \frac{\hat{Q}_1^2}{2C_{1\Sigma}} - E_J \cos\frac{2e}{\hbar}\hat{\Phi}_1 \tag{72}$$

where $C_{1\Sigma} \equiv C_J + C_{2s}$, and $\frac{1}{C_{2s}} \equiv \frac{1}{C_g} + \frac{1}{C_B}$. The linear resonator is simply a quantum harmonic oscillator with Hamiltonian

$$H_2 = \frac{\hat{Q}_2^2}{2C_{2\Sigma}} + \frac{\hat{\Phi}_2^2}{2L_B} \tag{73}$$

where $C_{2\Sigma} \equiv C_B + C_{1s}$, and $\frac{1}{C_{1s}} \equiv \frac{1}{C_g} + \frac{1}{C_J}$. Moreover, the interaction of the qubit and the resonator is captured in the coupling Hamiltonian

$$H_{12} = \frac{\beta}{C_{2\Sigma}}\hat{Q}_1\hat{Q}_2 \tag{74}$$

where $\beta \equiv \frac{C_g}{C_g + C_J}$ is calculated in [14] through electrostatic analysis. $\hat{Q}_1\hat{Q}_2$ indicates that coupled quantities are charges in nodes 1 and 2. The total Hamiltonian is

$$H = H_1 + H_2 + H_{12} \tag{75}$$

We can calculate the bare qubit eigenstates which are decoupled from the resonator using the qubit Hamiltonian only, H_1. The eigenstates are denoted as $|j\rangle$, and they can be calculated through the eigenvalue equation

$$H_1 |j\rangle = \epsilon_j |j\rangle \tag{76}$$

We can write the matrix elements of the charge operator as $Q_{1,jk} = \langle j | \hat{Q}_1 | k \rangle$. Then, the charge operator at node

1 is

$$\hat{Q}_1 = \sum_{j,k} Q_{1,jk} |j\rangle \langle k| \qquad (77)$$

Furthermore, the LC resonator Hamiltonian upon quantization is written as

$$H_2 = \hbar\omega_r \hat{a}^\dagger \hat{a} \qquad (78)$$

where $\omega_r = 1/\sqrt{L_B C_{2\Sigma}}$. Writing the charge operator at node 2 in terms of creation and annihilation operators, we obtain

$$\hat{Q}_2 = -iQ_{2ZPF}(\hat{a} - \hat{a}^\dagger) \qquad (79)$$

where $Q_{2ZPF} = \sqrt{\frac{C_B \hbar \omega_r}{2}}$. Upon plugging in all these expressions, the qubit-resonator coupling Hamiltonian becomes

$$H_{12} = -i\frac{\beta}{C_{2\Sigma}}Q_{2ZPF}\sum_{j,k} Q_{1,jk} |j\rangle \langle k| (\hat{a} - \hat{a}^\dagger) \qquad (80)$$

Finally, we can then write the total Hamiltonian as

$$H = \hbar\omega_r \hat{a}^\dagger \hat{a} + \sum_k \epsilon_k |k\rangle \langle k|$$
$$- i\frac{\beta}{C_{2\Sigma}}Q_{2ZPF}\sum_{j,k} Q_{1,jk} |j\rangle \langle k| (\hat{a} - \hat{a}^\dagger) \qquad (81)$$

Recall that transmon qubit is an anharmonic oscillator, but it is actually only weakly anharmonic. If were to assume that the qubit is sufficiently anharmonic, which is indeed an appropriate assumption as long as the qubit drive is properly calibrated, the qubit remains in the two-level computational subspace all the time. Hence, we can limit our analysis to two levels, and use the Pauli Z operator. With that, one can write

$$|0\rangle \langle 0| = \frac{1 - \sigma_z}{2} \qquad (82)$$

Further, for the raising and lowering operators of the qubit, we have

$$|1\rangle \langle 0| = \sigma_+ \qquad (83)$$

$$|0\rangle \langle 1| = \sigma_- \qquad (84)$$

$$|1\rangle \langle 1| = \frac{1 + \sigma_z}{2} \qquad (85)$$

Then, the total Hamiltonian consisting of the two-level artificial atom, linear resonator, and their coupling becomes

$$H = \hbar\omega_r \hat{a}^\dagger \hat{a} + \frac{\hbar\omega_{01}}{2}\sigma_z - i(\hat{a} - \hat{a}^\dagger)\hbar(g_{01}\sigma_- + g_{10}\sigma_+) \qquad (86)$$

where the coupling strength is

$$g_{ij} \equiv \frac{1}{\hbar}[\beta Q_{2ZPF}Q_{1,jk}/(C_{2\Sigma})] \qquad (87)$$

and we can assume that the static terms are zero, and only the transition elements are nonzero, $g_{00} = g_{11} = 0$. This is because the qubit has charge parity symmetry, $H(\hat{Q}) = H(-\hat{Q})$, which leads to $Q_{00} = \langle 0| \hat{Q} |0\rangle = 0$ and $Q_{11} = \langle 1| \hat{Q} |1\rangle = 0$. In other words, static dipole moments vanishes [14], whereas $g_{01} = g_{10} = g$. We can then write the Hamiltonian to be

$$H = \hbar\omega_r \hat{a}^\dagger \hat{a} + \frac{\hbar\omega_{01}}{2}\sigma_z - i\hbar g(\hat{a} - \hat{a}^\dagger)(\sigma_+ + \sigma_-) \qquad (88)$$

We can eliminate the energy non-conserving terms through the secular approximation (rotating wave approximation). As a result, we have

$$H = \hbar\omega_r \hat{a}^\dagger \hat{a} + \frac{\hbar\omega_{01}}{2}\sigma_z - i\hbar g(\hat{a}\sigma_+ - \hat{a}^\dagger\sigma_-) \qquad (89)$$

With the unitary transformation $U = e^{i\frac{\pi}{4}\sigma_z}$ such that $U\sigma_+ U^\dagger = i\sigma_+$, and $U\sigma_- U^\dagger = -i\sigma_-$ [14],

$$H = \hbar\omega_r \hat{a}^\dagger \hat{a} + \frac{\hbar\omega_{01}}{2}\sigma_z + \hbar g(\hat{a}\sigma_+ + \hat{a}^\dagger\sigma_-) \qquad (90)$$

which is indeed the Jaynes-Cummings Hamiltonian which lies at the heart of circuit QED [19, 20].

F. Qubit Readout

Having derived the Jaynes-Cummings Hamiltonian, we now have the machinery to calculate the dispersive regime Hamiltonian which enables the most popular way of reading out superconducting qubit state. Dispersive regime is the parameter regime with $\Delta \gg g$ where Δ is the detuning between the resonator and the qubit, $(\Delta \equiv \omega_{01} - \omega_r)$. In this way, qubit state can be read out in a non-destructive manner, meaning the qubit state remains the same after the measurement. It is important to note that the interaction $\hbar g(\hat{a}\sigma_+ + \hat{a}^\dagger\sigma_-)$ preserves the number of excitations, since we see that either the qubit is excited and a microwave photon is annihilated in the resonator, or the qubit is deexcited and a microwave photon is created in the resonator, which means the states $|g, n\rangle$ and $|e, n - 1\rangle$ couple only. In this notation, g and e refer to the ground and excited states of the qubit, and n refers to the number of microwave photons in the resonator. We further note that the coupling strength for the n-excitation manifold is

$$\langle e, n - 1| g(\hat{a} |e\rangle \langle g| + \hat{a}^\dagger |g\rangle \langle e|) |g, n\rangle = g\sqrt{n} \qquad (91)$$

Then, we can diagonalize the Hamiltonian, and calculate the eigenenergies at the n-excitation manifold. In the dispersive limit where $\Delta \gg g$, one obtains an expression for the eigenenergies as

$$E_{n\pm} = n\hbar\omega_r \pm \hbar\frac{\Delta}{2} \pm \hbar\frac{g^2}{\Delta}n \qquad (92)$$

As a natural result, we can then write the effective Hamiltonian in the dispersive regime as

$$H_{dispersive} = \hbar\omega_r \hat{a}^\dagger \hat{a} + \frac{1}{2}\hbar\Delta\sigma_z + \hbar\frac{g^2}{\Delta}\hat{a}^\dagger \hat{a}\sigma_z \qquad (93)$$

Another equivalent way to write this dispersive regime Hamiltonian is

$$H_{dispersive} = \hbar\left(\omega_r + \frac{g^2}{\Delta}\sigma_z\right)\hat{a}^\dagger \hat{a} + \frac{1}{2}\hbar\Delta\sigma_z \qquad (94)$$

where we see that there is a shift in the resonator frequency $(\pm\frac{g^2}{\Delta})$ depending on the qubit state which is called the dispersive shift [21]. Here, we see that one can measure the qubit state by simply measuring the cavity frequency, which is a quantum nondemolition measurement [20, 22]. Vector Network Analyzer measurement will simply show two distinct spectra depending on the qubit state, which can be seen in Fig. 6 (a). We can also infer the qubit state from the phase response, as shown in Fig. 6 (b).
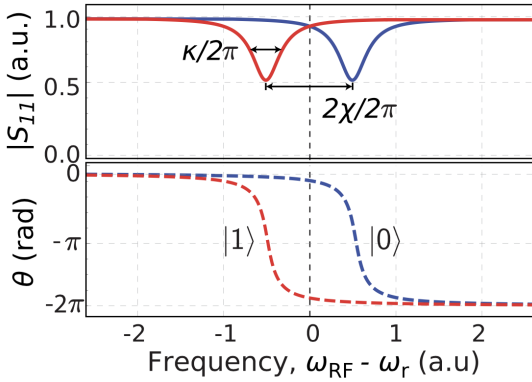

FIG. 6. Qubit state dependent shift in the readout resonator resonance frequency and phase. Figure taken from [18].

The final remark to note regarding the dispersive readout of transmon qubits in the circuit QED picture is that there is a correction to the dispersive shift term we derived $(\pm\frac{g^2}{\Delta})$ for a two-level artifical atom coupled to a linear resonator. This is because the transmon qubit is only weakly anharmonic. Thus, one has to take the higher excited state into account, and calculate the correction to the dispersive shift. One ends up with the expression [23]

$$\chi = -\frac{g^2}{\Delta}\frac{\alpha}{\Delta - \alpha} \qquad (95)$$

where α is the anharmonicity. Note that one recovers g^2/Δ in the limit of large anharmonicity.

In summary, we can perform the superconducting qubit state readout in circuit QED with microwave input near the cavity frequency through qubit state dependent dispersive shift [14].

V. CHALLENGES IN STATE-OF-THE-ART SUPERCONDUCTING QUBIT RESEARCH

There has been extensive study to characterize and mitigate the loss and noise problem in superconducting qubits. To name several decay channels, there are spontaneous emission, dielectric losses [24], quasiparticle tunneling due to broken Cooper pairs [25, 26], and coupling to spurious modes. These decay channels lower the T_1 by allowing the qubit to relax its energy into its environment [15].

On the other hand, dephasing time (T_2) is affected by the $1/f$ noise [27]. For instance, charge noise [28], flux noise [29], critical current noise [30] are dephasing channels for the superconducting qubit.

Here, we shall focus on the limiting factor for superconducting qubit lifetime, which are the two-level system defects.

A. Limiting Factor For Superconducting Qubit Lifetime

Although there has been significant improvement in the superconducting qubit lifetime over the years, it has been more or less stuck at around a few hundred microseconds recently [27]. This limitation has been mainly attributed to the two-level system defects (TLS) that emerge from deviation from the crystalline order. Since superconducting qubits are made with conventional micro and nanofabrication technologies, there are imperfect material interfaces, photoresists residuals due to lithography steps, structural damage due to etch steps, and surface oxides etc., all of which lead to amorphous layers with dangling bonds, hydrogen rotors, collective motion of atoms, etc. where TLSs reside. Microscopic nature of TLSs is not very well understood at the moment. However, there is a phenomenological model, known as the Standard Tunneling Model, where there is a double potential well modelling the two eigenstates of TLSs, which is shown in Fig. 7. In this model, TLSs can tunnel from
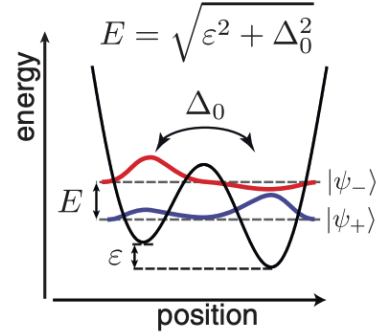

FIG. 7. Standard Tunneling Model with double-well potential. Figure taken from [31].

one configuration to the other with a tunneling energy of

Δ_0, and the two levels are separated with an asymmetry energy ε. The Hamiltonian for a TLS can be written as

$$H_{TLS} = \frac{1}{2} \begin{pmatrix} \varepsilon & \Delta_0 \\ \Delta_0 & -\varepsilon \end{pmatrix} \qquad (96)$$

Diagonalizing H_{TLS}, and calculating the eigenenergies give a TLS resonance of $E = \sqrt{\varepsilon^2 + \Delta_0^2}$. Then, we can write the Hamiltonian in the basis of eigenstates as

$$H_{TLS} = \frac{1}{2} E \sigma_z \qquad (97)$$

Therefore, these defects can resonantly absorb energy, and give rise to dielectric loss. Another remark to note is that the asymmetry energy ε depends on the environmental strain and electric fields, since TLSs have acoustic and electric dipole moment, which allow them to couple to strain and electric field in their environment, respectively. Asymmetry energy can be written as

$$\varepsilon = 2\vec{\gamma} \cdot \vec{S} + 2\vec{p} \cdot \vec{E} + \varepsilon_0 \qquad (98)$$

where $\vec{\gamma}$, $\vec{p}$, ε_0 are acoustic dipole, also known as deformation potential, electric dipole, and a static asymmetry term, respectively.

As a result of the coupling mechanism just mentioned above, TLSs lead to enhanced decay rate for the superconducting qubits, or equivalently reduced lifetime. In Fig. 8 (a), qubit frequency as a function of external magnetic flux is shown. Fig. 8 (b) shows the decay of the qubit in time domain. More importantly, we see in Fig. 8 (c) that when the qubit is tuned to be near resonance with an individual TLS, the superconducting qubit experiences enhanced decay rate. Each peak in the spectrum corresponds to a random TLS with different resonance frequency.

B. Efforts In The Literature

Having discussed the TLS-induced enhanced decay rate for superconducting qubits in the previous subsection, we shall now review what methods have been proposed in the literature to overcome this problem. To begin with, one way to remove TLS losses is removing lossy interfaces away from the high electric field regions [33, 34]. The idea behind this is that one can reduce the participation of lossy interfaces, such as substrate-metal and substrate-vacuum interfaces. On the other hand, it is known that metal-vacuum interface is less lossy. If one engineers a microwave circuit design with smaller portion of the electric field interacting with the lossy interfaces, TLS-induced loss decreases. This is because the coupling strength of TLSs is proportional to the electric dipole moment and electric field strength. Here, electric field strength is reduced at lossy interfaces by careful microwave engineering so that the coupling is weaker; hence, loss is lower. A similar idea is etching deep trenches into the substrate in fabrication so
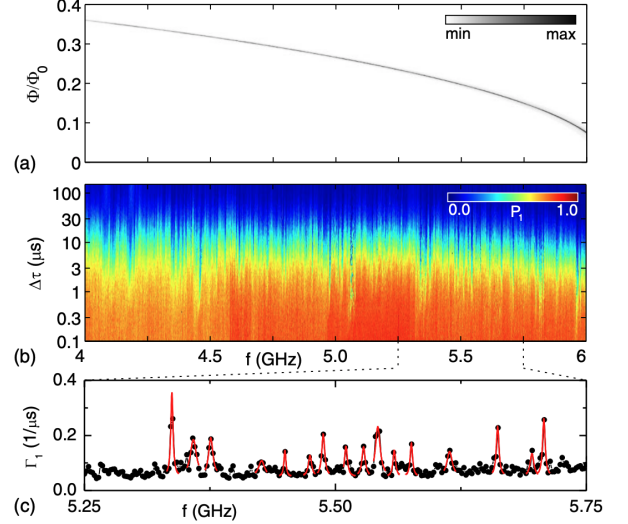

FIG. 8. (a) Qubit spectroscopy by frequency tuning through external magnetic flux applied. (b) Time-domain spectroscopy showing the decay of qubit population. (c) Qubit relaxation rate spectrum. Figure taken from [32].

that lossy interfaces are pushed far away from the high electric field regions [35]. Furthermore, there is effort in using 2D materials as capacitor dielectric, as they have very little TLS density, enabling higher quality factor superconducting circuits [36]. Since TLSs emerge from deviations from the crystalline order, material improvements enable less loss through smaller TLS density. In particular, adoption of crystalline dielectrics instead of amorphous layers improves the lifetime of superconducting qubits [37]. Moreover, surface passivation and treatment as a post-fabrication step lower the TLS-induced loss. In [38], nitrogen surface passivation was performed, achieving lower loss.

One remarkable achievement that has recently been shown is that superconducting qubits whose microwave circuits are made from tantalum perform better with a T1 time exceeding 0.3 ms [39]. This is because the native oxide of tantalum, TaOx, is less lossy, compared with commonly used superconductors, such as aluminum and niobium, indicating the state-of-the-art superconducting qubit research benefits from materials science and surface characterization significantly. In addition, thorough surface cleaning and characterizing surface level structure help improve the superconducting qubit lifetime and microwave resonator quality factors [40].

Another approach is studying novel qubit architectures with larger anharmonicity and noise protection. While larger anharmonicity enables faster control pulses, noise protection can improve the lifetime and coherence. To exemplify, capacitively shunted flux qubit [41] and fluxonium qubits [42] can achieve higher anharmonicity, whereas $0-\pi$ qubit is topologically noise protected [43].
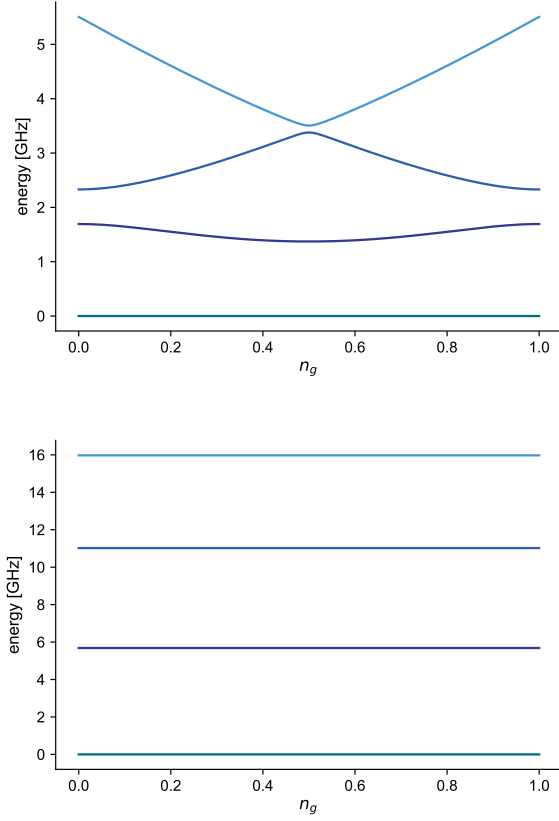
Appendix A: Transmon Energy Level Simulation

FIG. 9. Lowest 4 energy levels calculated by numerical analysis with varying offset charge n_g. Upper and lower figures depict the parameter regimes with $E_J/E_C = 5$ and $E_J/E_C = 50$, respectively. Figures are generated using scQubits Python package [16].

[1] Y. Nakamura, Y. A. Pashkin, and J. Tsai, Coherent control of macroscopic quantum states in a single-cooper-pair box, nature **398**, 786 (1999).

[2] J. Bardeen, L. N. Cooper, and J. R. Schrieffer, Microscopic theory of superconductivity, Physical Review **106**, 162 (1957).

[3] M. Tinkham, *Introduction to superconductivity* (Courier Corporation, 2004).

[4] M. H. Devoret, A. Wallraff, and J. M. Martinis, Superconducting qubits: A short review (2004).

[5] V. Bouchiat, D. Vion, P. Joyez, D. Esteve, and M. H. Devoret, Quantum coherence with a single cooper pair, Physica Scripta **T76**, 165 (1998).

[6] A. Blais, R.-S. Huang, A. Wallraff, S. M. Girvin, and R. J. Schoelkopf, Cavity quantum electrodynamics for superconducting electrical circuits: An architecture for quantum computation, Physical Review A **69**, 10.1103/physreva.69.062320 (2004).

[7] R. J. Schoelkopf, A. A. Clerk, S. M. Girvin, K. W. Lehnert, and M. H. Devoret, Noise and measurement backaction in superconducting circuits: qubits as spectrometers of quantum noise, in *SPIE Proceedings*, edited by L. B. Kish, F. Green, G. Iannaccone, and J. R. Vig (SPIE, 2003).

[8] R. Barends, J. Kelly, A. Megrant, D. Sank, E. Jeffrey, Y. Chen, Y. Yin, B. Chiaro, J. Mutus, C. Neill, P. O'Malley, P. Roushan, J. Wenner, T. C. White, A. N. Cleland, and J. M. Martinis, Coherent josephson qubit suitable for scalable quantum integrated circuits, Physical Review Letters **111**, 10.1103/physrevlett.111.080502 (2013).

[9] S. Gustavsson, O. Zwier, J. Bylander, F. Yan, F. Yoshi-

hara, Y. Nakamura, T. P. Orlando, and W. D. Oliver, Improving quantum gate fidelities by using a qubit to measure microwave pulse distortions, Physical Review Letters **110**, 10.1103/physrevlett.110.040502 (2013).

[10] R. Barends, J. Kelly, A. Megrant, A. Veitia, D. Sank, E. Jeffrey, T. C. White, J. Mutus, A. G. Fowler, B. Campbell, Y. Chen, Z. Chen, B. Chiaro, A. Dunsworth, C. Neill, P. O'Malley, P. Roushan, A. Vainsencher, J. Wenner, A. N. Korotkov, A. N. Cleland, and J. M. Martinis, Superconducting quantum circuits at the surface code threshold for fault tolerance, Nature **508**, 500 (2014).

[11] N. T. Bronn, B. Abdo, K. Inoue, S. Lekuch, A. D. Córcoles, J. B. Hertzberg, M. Takita, L. S. Bishop, J. M. Gambetta, and J. M. Chow, Fast, high-fidelity readout of multiple qubits, Journal of Physics: Conference Series **834**, 012003 (2017).

[12] M. D. Reed, B. R. Johnson, A. A. Houck, L. DiCarlo, J. M. Chow, D. I. Schuster, L. Frunzio, and R. J. Schoelkopf, Fast reset and suppressing spontaneous emission of a superconducting qubit 10.48550/ARXIV.1003.0142 (2010).

[13] B. Abdo, K. Sliwa, L. Frunzio, and M. Devoret, Directional amplification with a josephson circuit, Physical Review X **3**, 10.1103/physrevx.3.031001 (2013).

[14] S. M. Girvin, Circuit qed: superconducting qubits coupled to microwave photons, Quantum machines: measurement and control of engineered quantum systems , 113 (2014).

[15] J. Koch, M. Y. Terri, J. Gambetta, A. A. Houck, D. I. Schuster, J. Majer, A. Blais, M. H. Devoret, S. M. Girvin, and R. J. Schoelkopf, Charge-insensitive qubit design derived from the cooper pair box, Physical Review A **76**, 042319 (2007).

[16] P. Groszkowski and J. Koch, Scqubits: a python package for superconducting qubits, Quantum **5**, 583 (2021).

[17] A. Blais, A. L. Grimsmo, S. M. Girvin, and A. Wallraff, Circuit quantum electrodynamics, Reviews of Modern Physics **93**, 025005 (2021).

[18] P. Krantz, M. Kjaergaard, F. Yan, T. P. Orlando, S. Gustavsson, and W. D. Oliver, A quantum engineer's guide to superconducting qubits, Applied physics reviews **6**, 021318 (2019).

[19] P. Meystre and M. O. Scully, *Quantum optics* (Springer, 2021).

[20] A. Blais, R.-S. Huang, A. Wallraff, S. M. Girvin, and R. J. Schoelkopf, Cavity quantum electrodynamics for superconducting electrical circuits: An architecture for quantum computation, Physical Review A **69**, 062320 (2004).

[21] A. Blais, S. M. Girvin, and W. D. Oliver, Quantum information processing and quantum optics with circuit quantum electrodynamics, Nature Physics **16**, 247 (2020).

[22] A. Wallraff, D. I. Schuster, A. Blais, L. Frunzio, R.-S. Huang, J. Majer, S. Kumar, S. M. Girvin, and R. J. Schoelkopf, Strong coupling of a single photon to a superconducting qubit using circuit quantum electrodynamics, Nature **431**, 162 (2004).

[23] P. Arrangoiz-Arriola, E. A. Wollack, Z. Wang, M. Pechal, W. Jiang, T. P. McKenna, J. D. Witmer, R. Van Laer, and A. H. Safavi-Naeini, Resolving the energy levels of a nanomechanical oscillator, Nature **571**, 537 (2019).

[24] J. M. Martinis, K. B. Cooper, R. McDermott, M. Steffen, M. Ansmann, K. Osborn, K. Cicak, S. Oh, D. P. Pappas, R. W. Simmonds, *et al.*, Decoherence in josephson qubits from dielectric loss, Physical review letters **95**, 210503 (2005).

[25] R. Lutchyn, L. Glazman, and A. Larkin, Quasiparticle decay rate of josephson charge qubit oscillations, Physical Review B **72**, 014517 (2005).

[26] R. Lutchyn, L. Glazman, and A. Larkin, Kinetics of the superconducting charge qubit in the presence of a quasiparticle, Physical Review B **74**, 064515 (2006).

[27] I. Siddiqi, Engineering high-coherence superconducting qubits, Nature Reviews Materials **6**, 875 (2021).

[28] B. Christensen, C. Wilen, A. Opremcak, J. Nelson, F. Schlenker, C. Zimonick, L. Faoro, L. Ioffe, Y. Rosen, J. DuBois, *et al.*, Anomalous charge noise in superconducting qubits, Physical Review B **100**, 140503 (2019).

[29] P. Kumar, S. Sendelbach, M. Beck, J. Freeland, Z. Wang, H. Wang, C. Y. Clare, R. Wu, D. Pappas, and R. McDermott, Origin and reduction of 1/f magnetic flux noise in superconducting devices, Physical Review Applied **6**, 041001 (2016).

[30] D. Van Harlingen, T. Robertson, B. Plourde, P. Reichardt, T. Crane, and J. Clarke, Decoherence in josephson-junction qubits due to critical-current fluctuations, Physical Review B **70**, 064517 (2004).

[31] C. Müller, J. H. Cole, and J. Lisenfeld, Towards understanding two-level-systems in amorphous solids: insights from quantum circuits, Reports on Progress in Physics **82**, 124501 (2019).

[32] R. Barends, J. Kelly, A. Megrant, D. Sank, E. Jeffrey, Y. Chen, Y. Yin, B. Chiaro, J. Mutus, C. Neill, *et al.*, Coherent josephson qubit suitable for scalable quantum integrated circuits, Physical review letters **111**, 080502 (2013).

[33] C. Wang, C. Axline, Y. Y. Gao, T. Brecht, Y. Chu, L. Frunzio, M. Devoret, and R. J. Schoelkopf, Surface participation and dielectric loss in superconducting qubits, Applied Physics Letters **107**, 162601 (2015).

[34] C. E. Murray, Material matters in superconducting qubits, Materials Science and Engineering: R: Reports **146**, 100646 (2021).

[35] A. Bruno, G. De Lange, S. Asaad, K. Van Der Enden, N. Langford, and L. DiCarlo, Reducing intrinsic loss in superconducting resonators by surface treatment and deep etching of silicon substrates, Applied Physics Letters **106**, 182601 (2015).

[36] J. I. Wang, M. A. Yamoah, Q. Li, A. H. Karamlou, T. Dinh, B. Kannan, J. Braumüller, D. Kim, A. J. Melville, S. E. Muschinske, *et al.*, Hexagonal boron nitride as a low-loss dielectric for superconducting quantum circuits and qubits, Nature materials **21**, 398 (2022).

[37] S. Weber, K. Murch, D. Slichter, R. Vijay, and I. Siddiqi, Single crystal silicon capacitors with low microwave loss in the single photon regime, Applied Physics Letters **98**, 172510 (2011).

[38] K. Zheng, D. Kowsari, N. Thobaben, X. Du, X. Song, S. Ran, E. Henriksen, D. Wisbey, and K. Murch, Nitrogen plasma passivated niobium resonators for superconducting quantum circuits, Applied Physics Letters **120**, 102601 (2022).

[39] A. P. Place, L. V. Rodgers, P. Mundada, B. M. Smitham, M. Fitzpatrick, Z. Leng, A. Premkumar, J. Bryon, A. Vrajitoarea, S. Sussman, *et al.*, New material platform for superconducting transmon qubits with coherence times exceeding 0.3 milliseconds, Nature communi-

cations **12**, 1779 (2021).

[40] K. D. Crowley, R. A. McLellan, A. Dutta, N. Shumiya, A. P. Place, X. H. Le, Y. Gang, T. Madhavan, N. Khedkar, Y. C. Feng, *et al.*, Disentangling losses in tantalum superconducting circuits, arXiv preprint arXiv:2301.07848 (2023).

[41] F. Yan, S. Gustavsson, A. Kamal, J. Birenbaum, A. P. Sears, D. Hover, T. J. Gudmundsen, D. Rosenberg, G. Samach, S. Weber, *et al.*, The flux qubit revisited to enhance coherence and reproducibility, Nature communications **7**, 12964 (2016).

[42] V. E. Manucharyan, J. Koch, L. I. Glazman, and M. H. Devoret, Fluxonium: Single cooper-pair circuit free of charge offsets, Science **326**, 113 (2009).

[43] P. Groszkowski, A. D. Paolo, A. Grimsmo, A. Blais, D. Schuster, A. Houck, and J. Koch, Coherence properties of the 0-πqubit, New Journal of Physics **20**, 043053 (2018).